A transcriptionally distinct CXCL13+CD103+CD8+ T-cell population is associated with B-cell recruitment and neoantigen load in human cancer

Workel, Hagma H; Lubbers, Joyce M; Arnold, Roland; Prins, Thalina M; van der Vlies, Pieter; de Lange, Kim; Bosse, Tjalling; Van Gool, Inge C; Eggink, Florine A; Wouters, Maartje Ca

Published in:
Cancer immunology research

DOI:
10.1158/2326-6066.CIR-18-0517

Publication date:
2019

Author Manuscript Published OnlineFirst on March 14, 2019; DOI: 10.1158/2326-6066.CIR-18-0517
Author manuscripts have been peer reviewed and accepted for publication but have not yet been edited.

A transcriptionally distinct CXCL13^{+}CD103^{+}CD8^{+} T-cell population is associated with B-cell recruitment and neoantigen load in human cancer

Hagma H. Workel[1,2], Joyce M. Lubbers[1,2], Roland Arnold[3], Thalina M. Prins[1], Pieter van der Vlies[4], Kim de Lange[4], Tjalling Bosse[5], Inge C. van Gool[5], Florine A. Eggink[1], Maartje C.A. Wouters[6], Fenne L. Komdeur[1], Elisabeth C. van der Slikke[1], Carien L. Creutzberg[7], Arjan Kol[1], Annechien Plat[1], Mark Glaire[8], David N. Church[8,9], Hans W. Nijman[1,10], Marco de Bruyn[1,10,*]

[1]University of Groningen, University Medical Center Groningen, Department of Obstetrics and Gynecology, The Netherlands

[2]Authors share first authorship

[3]Institute of Cancer and Genomic Sciences, University of Birmingham, Birmingham, United Kingdom

[4]University of Groningen, University Medical Center Groningen, Department of Genetics, The Netherlands

[5]Leiden University, Leiden University Medical Center, Department of Pathology, The Netherlands

[6]Trev and Joyce Deeley Research Centre, BC Cancer, Victoria, British Columbia, Canada

[7]Leiden University, Leiden University Medical Center, Department of Radiation Oncology, The Netherlands

[8]University of Oxford, Molecular and Population Genetics Laboratory, The Wellcome Trust Centre for Human Genetics and Oxford Cancer Centre, United Kingdom

[9]NIHR Oxford Biomedical Research Centre, Oxford University Hospitals NHS Foundation Trust, John Radcliffe Hospital, Oxford OX3 9DU

[10]Authors share senior authorship

***Corresponding author:**

Marco de Bruyn, PhD

University Medical Center Groningen

CMC V, 4e floor, room Y4.240

PO 30.001

9700 RB Groningen

Tel + 31 (0)50 3613174

Fax + 31 (0)50 3611806

Email m.de.bruyn@umcg.nl

Keywords: CXCL13, TGFβ1, tertiary lymphoid structures, CD103$^+$ T cell, immune checkpoint inhibitors

Running title: TGFβ induces CXCL13 in CD103$^+$ tumor-infiltrating T cells

Disclosure of Competing Interests: The authors have no conflicts of interest to disclose.

Abstract: 161

Text: 4645

4 Figures, 1 Table, 3 Supplementary Figures, 8 Supplementary Tables

Abstract

The chemokine CXCL13 mediates recruitment of B cells to tumors and is essential for the formation of tertiary lymphoid structures (TLSs). TLSs are thought to support antitumor immunity and are associated with improved prognosis. However, it remains unknown whether TLSs are formed in response to the general inflammatory character of the tumor microenvironment, or rather, are induced by (neo)antigen-specific adaptive immunity. We here report on the finding that the transforming growth factor beta (TGFβ)-dependent $CD103^+CD8^+$ tumor-infiltrating T-cell (TIL) subpopulation expressed and produced CXCL13. Accordingly, $CD8^+$ T cells from peripheral blood activated in the presence of TGFβ upregulated CD103 and secreted CXCL13. Conversely, inhibition of TGFβ receptor signaling abrogated CXCL13 production. $CXCL13^+CD103^+CD8^+$ TILs correlated with B-cell recruitment, TLSs, and neoantigen burden in six cohorts of human tumors. Altogether, our findings indicated that TGFβ plays a non-canonical role in coordinating immune responses against human tumors and suggest a potential role for $CXCL13^+CD103^+CD8^+$ TILs in mediating B-cell recruitment and TLS formation in human tumors.

Introduction

Immune checkpoint inhibitors (ICIs) targeting programmed death ligand 1 (PD-L1) or its receptor, programmed death 1 (PD-1), have elicited unprecedented long-term disease remissions in advanced and previously treatment-refractory cancers [1–3]. Unfortunately, only a subset of patients currently benefit from treatment. ICIs are more likely to be effective in patients with a pre-existing anti-cancer immune response, most notably a $CD8^+$ cytotoxic T-cell response against tumor neoantigens [4].

Responsive tumors harbor significantly more predicted neoantigens [5,6] and display evidence of a coordinated immune response comprising T cells, dendritic cells (DCs), and B cells [7]. In diseases that parallel tumor development, such as chronic inflammatory conditions, this coordinated infiltration by different immune cell subsets is frequently associated with tertiary lymphoid structures (TLSs) – an ectopic form of lymphoid tissue. TLSs exhibit features of regular lymph nodes, including high endothelial venules, a T-cell zone with mature DCs, and a germinal center with follicular DCs and B cells [8]. Several studies have reported the presence of TLSs in tumors, which was generally found to be associated with greater immune control of cancer growth and improved prognosis [9,10]. For several malignancies, the combination of TLS presence and high $CD8^+$ T-cell infiltration was found to associate with superior prognosis, whereas high $CD8^+$ T-cell infiltration alone associated with poor or moderate prognosis [11,12]. These observations highlight the importance of a coordinated immune response, including TLS formation, in anti-cancer immunity.

To date, the molecular determinants of tumor TLS formation remain incompletely understood. Current data suggest that TLS formation results from a complex interplay between DCs, T cells, B cells, and supporting stromal cells. Interplay amongst these cells relies on reciprocal cytokine and chemokine signaling, including chemokine [C-X-C motif] ligand 13 (CXCL13), receptor activator of nuclear factor κ B (ligand)(RANK/RANKL), lymphotoxin αβ (LTαβ), and chemokine (C-C motif) ligand 21 (CCL21) [13]. A central role for CXCL13 in this process is suggested by the inability of B cells to home and accumulate into lymphoid aggregates [14] and generate functional lymphoid tissue [15,16] in CXCL13-knockout mice and the observation that CXCL13 alone is sufficient to generate lymphoid tissues [17–19]. Nevertheless, a key outstanding question remains whether tumor-associated TLSs are formed in response to the general inflammatory character of the tumor microenvironment, or rather, are induced by (neo)antigen-specific adaptive immunity. Two studies suggest that a subset of

CXCL13-producing $CD8^+$ tumor-infiltrating lymphocytes (TILs) may link (neo)antigen recognition to TLS formation [20,21].

Here, we report the finding that transforming growth factor beta (TGFβ) receptor signaling licensed $CD8^+$ T cells to produce and secrete CXCL13 upon concurrent T-cell receptor (TCR) stimulation. Induction of CXCL13 was paralleled by upregulation of CD103, a marker for tissue-resident TILs. Accordingly, bulk and single-cell RNA sequencing identified exclusive expression of CXCL13 in human $CD103^+$, but not $CD103^-$, $CD8^+$ TILs. In line with these data, the presence of $CD103^+$ cytotoxic T lymphocytes (CTLs) correlated to B-cell recruitment and TLSs in tumors with a high mutational load. This discovery sheds light on how B cells could be recruited to tumors by CTLs, identifying a non-canonical role for TGFβ in the orchestration of a coordinated immune response against human (neo)antigen-rich tumors. Our findings also identify CD103 and B cells as potential biomarkers for ICI in epithelial malignancies.

Materials and Methods

Patients

Tumor tissue from four patients with stage IIIC high-grade serous ovarian cancer was collected during primary cytoreductive surgery, prior to chemotherapy, and from one patient with stage IV high-grade serous ovarian cancer during interval debulking upon three cycles of chemotherapy. Written informed consent was obtained from all patients. Selection of uterine cancer (UC) patients was described previously [22]. Briefly, UC tissue was obtained from patients involved in the PORTEC-1[23] and PORTEC-2[24] studies (n=57), the UC series (n=67) from Leiden University Medical Center (LUMC), and UC series (n=26) from the University Medical Center Groningen in accordance with local medical ethical guidelines [25]. Tumor material was fixed in formalin and embedded in paraffin. Tumor material from 119 patients was available for analysis. Mutations in the exonuclease domain of polymerase epsilon (*POLE*-EDM) and microsatellite instability status were known from previous studies [25]. Of the tumors available for this study, 42 tumors were *POLE* wild-type and microsatellite stable (MSS), 38 were *POLE* wild-type with microsatellite instability (MSI), and 39 were *POLE*-EDM. *POLE*-EDM statuses did not co-occur with microsatellite instability. All cases were of endometrioid histology (EEC), and the number of low-grade and high-grade tumors was spread equally over the

three molecular groups. Selection of ovarian cancer patients and CD103 staining was reported previously [26]. Ethical approval for tumor molecular analysis was granted at LUMC, UMCG, and by Oxfordshire Research Ethics Committee B (Approval No. 05\Q1605\66).

Analysis of TCGA mRNA sequencing data

RSEM normalized mRNA-seq data and clinical data from uterine corpus endometrial carcinoma (UCEC), ovarian cancer (OV), breast cancer (BRCA), and lung adenocarcinoma (LUAD) were downloaded from firebrowse.org on 13-03-2017 (UCEC) and 14-07-2017(OV, BRCA, LUAD). RSEM mRNA sequencing expression data were log2 +1 transformed, and genes with zero reads in all samples were removed. *POLE*-EDM, MSI and MSS cases were identified in the endometrial cancer data. The mononucleotide and dinucleotide marker panel analysis status was provided by The Cancer Genome Atlas (TCGA), and mutations in the exonuclease domain of *POLE* were determined previously [27]. Heatmaps were constructed in R (version 3.3.1) with packages gplots and ggplots. The gene set of TLSs was reported previously [10,28]. Gene sets for the $CD8^{+}CD103^{+}$ and $CD8^{+}CD103^{-}$ signatures were derived from the sequencing data (**Supplementary Table S1**). Spearman correlations between the TLS signature, the $CD8^{+}CD103^{+}$ signature, and the $CD8^{+}CD103^{-}$ signature were visualized in correlation plots using the Corrplot package (Version 0.77) in R. $CXCL13^{high}CD103^{high}$ versus $CXCL13^{low}CD103^{low}$ groups in MSS UCEC were based on median expression of *CXCL13* (4.35698) and *ITGAE* (8.086985). Survival curves were constructed with R packages survival (version 2.41-3) and survminer (version 0.4.3). All analyses were performed in R (version 3.4.0), with exception of the construction of the heatmap in Figure 3C, which was made in R version 3.3.1.

Immunohistochemistry

To assess the presence of TLSs in UC, we stained for the B cell marker CD20 on whole tissue sections. Formalin-fixed, paraffin-embedded (FFPE) slides were de-paraffinized and rehydrated in graded ethanol. Antigen retrieval was initiated with a preheated 10 mM citrate buffer (pH=6) and endogenous peroxidase activity was blocked by submerging sections in a 0.45% hydrogen peroxide

solution. Slides were blocked in PBS containing 1% human serum and 1% BSA. Slides were incubated overnight with anti-CD20 (0.63 mg/L; clone L26, cat. number M0755, Dako, Glostrup, Denmark) at 4°C. Subsequently, slides were incubated with a ready-to-use peroxidase-labeled polymer for 30 minutes (Envision+/HRP anti-mouse, 2 drops, cat. number K4001, Dako, Carpinteria, USA). Signal was visualized with 3,3'diaminobenzidin (DAB) solution, and slides were counterstained with hematoxylin. Appropriate washing steps with PBS were performed in-between incubation steps. Sections were embedded in Eukitt mounting medium (Sigma Aldrich, Steinheim, Germany), and slides were scanned on a Hamamatsu digital slide scanner (Hamamatsu photonics, Hamamatsu, Japan). The number of $CD20^+$ (dense) follicles in each slide was quantified in NDPview2 software by two independent observers who were blinded to clinicopathological data.

Immunohistochemistry for CD8 was performed previously in this cohort [25]. To assess the survival effect of CD103 infiltration in mismatch repair proficient (pMMR) cancers, we used a staining for CD103 on tissue microarray slides of UC [29]. FFPE slides were prepared as described above and incubated with rabbit-anti human CD103 (1 mg/L; anti-E7-integrin, clone ERPR4166(2), cat. number Ab129202, Abcam, Cambridge UK), followed by a ready-to-use peroxidase-labeled polymer (Envision+/HRP anti-rabbit, cat.no. K4003, Dako, Carpinteria, USA) and Biotin Tyramide working solution (TSA kit, Perkin Elmer, Waltham, USA), streptavidin-HRP (TSA kit, Perkin Elmer), and 3,3'-diaminobenzidin/hematoxylin. Positively stained cells were quantified per core and adjusted for core surface. Patients with at least two cores with a minimum of 20% tumor epithelium were included for analysis. All slides were counted manually by two individuals who were blinded for clinicopathological data.

Multi-color immunofluorescence

FFPE slide preparation and antigen retrieval were performed as described above. Next, slides were incubated overnight at 4°C with primary antibody and subsequently incubated with the appropriate secondary antibody for 45 minutes at room temperature (**Supplementary Table S2**). Specific signal was amplified using the TSA Cyanine 5 (Cy5) detection kit (Perkin Elmer, NEL705A001KT, Boston, USA) or the TSA Cyanine 3 (Cy3) and Fluorescein detection kit (Perkin Elmer, 753001KT, Waltham, USA), according to manufacturer's protocols. To allow multiple amplifications on the same slide,

primary HRP labels were destroyed between incubations by washing with 0.01 M hydrochloric acid for 10 minutes. Appropriate washing steps with PBS containing 0,.05% Tween20 (Sigma-Aldrich, Missouri, USA) were performed during the procedure. For embedding, Prolong Diamond anti-fade mounting medium with or without DAPI was used (Invitrogen/Thermo Fisher Scientific, P36962 and P36961, Oregon, USA). Finally, slides were scanned at room temperature using the TissueFAXS acquisition software and microscope (TissueGnostics, Vienna, Austria) with the following specifications: Zeiss EC "Plan-Neofluar" 40x/1.30 Oil, DIC objective, CMOS-color camera PL-B623 Pixelink (3.1 Megapixels), EXFO Excite 120 PC fluorescence illumination and Chroma ET Dapi (49000), Chroma ET CY3 (49004), Chroma ET Cy5 (49006), and Chroma FITC (49011) filter sets. Overlay images were produced using Adobe Photoshop software.

mRNA sequencing

Ovarian tumors from two patients were cut into pieces of <1 mm^3 and placed in a T75 culture flask (Nunc™ EasYFlask™ Cell Culture Flasks, cat. no. 156499, ThermoScientific) with digestion medium, consisting of RPMI (Gibco, Paisley, UK), 10% fetal bovine serum (FBS, Gibco, Paisley, UK), collagenase type IV (1 mg/mL; Gibco, Grand Island, USA), and recombinant human DNase (12.6 µg/mL; Pulmozyme,Roche, Woerden, the Netherlands) for overnight digestion at room temperature. After digestion, the suspension was strained through a 70 µm filter and washed with PBS. Cells were centrifuged over a Ficoll-Paque gradient (GE Healthcare Bio-Sciences AB, Uppsala, Sweden), and lymphocytes were isolated from between the two layers. After a wash with PBS cells were pelleted. Total cell pellet was suspended in 1mL FBS with 10% dimethylsulfoxide (Merck, Darmstadt, Germany), and stored in liquid nitrogen until further use.

Prior to sequencing, tumor digests were thawed on ice, washed with AIM-V medium (Gibco, Paisley, UK) with 5% pooled human serum (PHS, One Lambda, USA) and centrifuged at 1000 x *g*. The total cell pellets were resuspended in AIM-V with 5% PHS, and cells were incubated with CD3-BV421, CD4-PerCP-Cy5.5, CD8α-APCeFluor780, CD8β-PEcy7, TCRαβ-APC, CD103-FITC, and CD56-PE antibodies at 4°C for 45 minutes (**Supplementary Table S3**). After gating for $CD3^+CD4^-$ $CD8\alpha\beta^+TCR\alpha\beta^+CD56^-$ cells, $CD103^-$ and $CD103^+$ single cells were sorted on a Beckman Coulter Astrios cytometer directly into 4 µL lysis buffer (2 µL of 0.2% Triton X-100, Sigma-Aldrich, cat. no.

T9284) with 5% recombinant RNase inhibitor (Westburg-Clontech, cat. no. 2313A), 1 µL of 10µM barcoded oligo dT primer, and 1 µL 4x10 mM dNTP mix in 96-well PCR plates. Each well contained a unique indexed Oligo dT primer (custom designed by P. van der Vlies, **Supplementary Table S4**, enabling identification of individual cells after pooled RNA sequencing.

In addition to single cell wells, small bulk populations of 20 cells were sorted per microplate well. Per patient, 40 single $CD8^+$ T cells (20 wells $CD103^+$, 20 wells $CD103^-$) and 20 small bulk 20-cell populations (10 wells $CD103^+$, 10 wells $CD103^-$) were sorted. After sorting, the plate was vortexed and spun down briefly, and incubated at 72°C for 3 minutes. After this step the plate was kept cool. The transcriptomes were amplified by a modified SMART-Seq2 protocol using SmartScribe reverse transcriptase (Westburg-Clontech, CL639537), based on a previously published protocol [30]. In brief, custom primers were designed that included a PCR-primer recognition site for pre-PCR, a Unique Molecular Identifier (UMI), a cell barcode (see **Supplementary Table S4**), and a poly T-stretch. Each cell (or pool) was tagged with an oligo dT primer, including the UMI and cell barcode. A template switching pre-PCR was used t o generate cDNA. Pools are made of single cells or pools with unique cell barcodes and 500 pg of the pools was tagmentated and barcoded using a N7xx index and custom P5 hybrid primer: (AATGATACGGCGACCACCGAGATCTACACGCCTGTCCGCGGAAGCAGTGGTATCAACGCAGAG T*A*C) according the Illumina Nextera XT DNA sample preparation kit protocol (Illumina, cat. no. FC-131-1096). The pools were purified using AMPure beads, in a ratio of 0.6:1, to remove primer dimers. Presence and size distribution of the obtained PCR product were checked on a PerkinElmer LabChip GX high-sensitivity DNA chip. A super pool was created by equimolar pooling (1 nmol/L) of the Nextera products, and the samples were sequenced on Illumina NextSeq500 2500 using 50 bp paired-end reads, one read for the mRNA transcript, and the other for the cell-barcode. The obtained RNA sequencing data were demultiplexed into individual FASTQ files. The obtained single-end reads were aligned to human reference genome 37 (GRCh37.p13 (GCA_000001405.14), top-level built) using STAR (version 2.5.2).

RNA-SeQC (version 1.1.8) was then used to assess the quality of single cells. Data were visualized, and clear low-quality outliers were identified based on the number of transcripts, uniquely mapped reads, mapping rate, expression profiling efficiency and exonic rate, and these were removed from

further analysis. All cells that did not meet one of the following criteria were removed: <10000 transcripts detected, <500000 uniquely mapped reads, <1000 genes detected, a mapping rate of <0.5, an expression profiling efficiency of <0.4, or an exonic rate of <0.5 (**Supplementary Table S5**). mRNA expression values for single cells are shown in fragments per kilobase million (FKPM) and log2+1 transformed. Differential expression in the 20-cell populations was analyzed with DESeq2 (version 1.16.1) to obtain insight into the differences between $CD103^+$ and $CD103^-$ $CD8^+$ T cells. For this analysis, expression values for each sample have been obtained using RSEM (version1.3.0, with Bowtie 2, version 2.2.5, non-stranded and with the single-cell prior activated to account for drop-out genes) and have been computed for the Gencode 19 transcriptome annotation for GRCh37 (reference index built with –polyA activated). Genes with a Benjamini-Hochberg FDR <0.01 and log2 fold change >1 were selected for further analysis. Differentially expressed genes were visualized in a Volcano plot (DESeq2, version 1.16.1). The accession number for the sequencing data reported in this study is GSE127888.

ELISA

TILs from three high-grade serous ovarian cancer digests were stained and sorted as described for mRNA sequencing. The number of sorted T cells for the three patients were 163 $x10^3$, 216 $x10^3$, and 154 $x10^3$ for $CD4^+$ cells; 82 $x10^3$, 38$x10^3$, and 83 $x10^3$ for $CD8^+CD103^-$; and 207 $x10^3$, 120 $x10^3$, and146 $x10^3$ for $CD8^+CD103^+$ T cells. Sorted T cells remained unstimulated or were activated either with a stimulation cocktail containing phorbol myristate acetate (PMA, 40.5µM) and ionomycin (670µM, 500x dilution, Invitrogen, 00-4970-93 Carlsbad USA) or with Dynabeads® (2 µL/1$x10^5$ cells, T-activator CD3/CD28 beads, 11131D, Gibco, Oslo, Norway and Vilnius, Lithuania).

Peripheral blood $CD8^+$ T cells were isolated from blood of four healthy volunteers (Sanquin, written informed consent was obtained) by a Ficoll-Paque gradient followed by magnetic activated cell sorting with a $CD8^+$ T-cell negative selection kit (purity >90%, MagniSort™ Human CD8 T cell Enrichment Kit, cat. no. 8804-6812-74; Thermo Scientific, San Diego, USA). Peripheral blood $CD8^+$ T cells were incubated in 100 µL AIM-V medium with or without Dynabeads® (2 µL/1$x10^5$ cells) for activation, recombinant TFGβ1 (rTGF- β1, 100 ng/mL, Peprotech, USA), TGFβ1 receptor inhibitor (10 µM, SB431542, Sigma Aldrich/Merck, Saint Louis, USA), or a combination of these. Similar experiments

were performed with the addition of IL2 (100 IU/mL. Novartis Pharmaceuticals, UK). For the dose-response curve, peripheral blood $CD8^+$ T cells from three healthy donors were incubated with or without Dynabeads® (2µL/1x10^5 cells) for activation and with recombinant TFGβ1 at doses ranging from 0 to 100 ng/mL (rTGF β1, Peprotech, USA). All cells were cultured in AIM-V medium with 5% pooled human serum (cat.no. A25761, One Lambda, Los Angeles, USA) in 96-well plates containing 1x10^5 cells per condition. After 7 days, plates were centrifuged and supernatant was collected for ELISA.

CXCL13 sandwich ELISA experiments were performed according to manufacturer's protocol (Human CXCL13/BLC/BCA-1 DuoSet ELISA DY801, R&D Abingdon, UK or, for the dose-response curve, Minneapolis, USA). In brief, Nunc MaxiSorp flat-bottom plates (Invitrogen, Carlsbad, USA) were coated with a capture antibody, followed by incubation with cell supernatant. Per condition, 70 µL of supernatant was diluted with 40 µL 1% BSA in PBS, after which 100 µL was added to the well. Binding of CXCL13 was detected using secondary antibody, streptavidin-HRP and TMB 1-Component Microwell Peroxidase Substrate (SureBlue, KPL/SeraCare, Milford, USA). Substrate conversion was stopped after 20 minutes with 0.01 M hydrogen chloride. Plates were washed with PBS plus 0.05% Tween20 in-between incubations. OD values were obtained using a micro plate reader set to 450 nm (BioRad iMark™ Microplate reader). Lastly, the derived CXCL13 concentrations (pg/mL) were multiplied by 1.57 to correct for diluting. AIM-V medium only was used as a negative control.

Chemokine arrays

$CD8^+$ T cells were isolated from blood of three healthy donors as described above in the ELISA section. Per condition, 5x10^5 cells were cultured in AIM-V medium with 5% PHS in a 24-well plate. Cells were either incubated for 7 days in medium alone, with rTGFβ1 (100 ng/mL, Peprotech, USA), with Dynabeads® (2 µL/1x10^5 cells, T-activator CD3/CD28 beads, 11131D, Gibco, Oslo, Norway and Vilnius, Lithuania), or with both rTGFβ1 and Dynabeads®. Samples were centrifuged, and supernatants were collected to analyze production of chemokines on chemokine arrays, according to manufacturer's instructions (31 chemokines using the Proteome Profiler Human Chemokine Array Kit, ARY017, R&D, Abingdon, UK, and 38 chemokines using the Human Chemokine Antibody Array - Membrane, ab169812, Abcam, Huissen, the Netherlands) (**Supplementary Table S6**). In brief,

chemokine receptor-coated membranes were incubated with supernatant overnight at 4°C. Per condition, 450 µL of supernatant was diluted with 1050 µL buffer, provided by the supplier, and 1500 µL was added (R&D), or 1000 µL was added undiluted (Abcam). Captured proteins were visualized using chemiluminescent detection reagents, provided by the suppliers. Appropriate washing steps using wash buffers provided by the suppliers were performed in-between incubation steps. Membranes were imaged on the BioRad ChemiDoc^{TM} MP Imaging System, and densitometric analysis of chemokine spots was performed using the Protein Array Analyzer plugin for Image J [31].

Statistical analyses

Differentially expressed genes in $CD103^{+}CD8^{+}$ versus $CD103^{-}CD8^{+}$ T cells sorted from human ovarian tumors were determined by DESeq2 for 20 cell-populations. Genes with a Benjamini-Hochberg FDR <0.01 and log2 fold change >1 were selected for further analysis. Differences in FPKM-values of single cells were assessed by a Mann-Whitney U test. Differences in number of $CD20^{+}$ follicles on FFPE slides of molecular subgroups of EC were determined by a non-parametric Kruskal-Wallis test, followed by Dunn's post-hoc analysis. We analyzed the TCGA mRNA sequencing data and compared differences in gene expression between molecular subgroups of EC with a non-parametric Kruskal-Wallis test and a post-hoc Dunn's test. Differences in survival were determined by a logrank test. CXCL13 production was analyzed using a Kruskal-Wallis comparison with a post-hoc Dunn's test, or, for the dose-response curve, with a two-way ANOVA followed by a post-hoc Bonferroni test. The chemokine arrays were analyzed using a Kruskal-Wallis test with a post-hoc Dunn's test. The survival effect of CD103 in pMMR UC was assessed by Kaplan Meier analysis and logrank test by comparing 'above median CD103 expression' and 'equal to or below median CD103 expression' (cut-off 16.14) patient groups. Uni- and multivariate analyses were performed by disease-specific cox regression survival analyses (Enter for univariate and Backward and Forward (both LR and conditional) methods for multivariate analyses). All statistical analyses were performed using R version 3.4.0 or GraphPad Prism (GraphPad Software Inc., CA, USA). A p-value of <0.05 was used as a cut-off for significance.

Results

Epithelial CD8+ T cells associate with an activated and exhausted transcriptional signature

We and others have previously shown that intraepithelial CD103$^+$, but not stromal CD103$^-$, CD8$^+$ TILs are promising targets for ICI therapy [26,32–34]. To understand the underlying transcriptional changes in these two cell populations, we performed mRNA sequencing on single- and 20-cell pools of CD8$^+$ T cells isolated from human tumors. We chose ovarian cancer as a model tumor because of its large tumor bulk, availability of pre-treatment tissue, and a high number of distinct CD103$^+$ and CD103$^-$ infiltrating CD8$^+$ cells. CD8$^+$ TILs were defined based on a CD3+/TCRαβ+/CD8αβ+/CD56-/CD4- phenotype (**Fig. 1A**). Post hoc t-distributed stochastic neighbor embedding (t-SNE) confirmed the presence of unique CD103$^+$ and CD103$^-$ CTL populations in these tumors (**Supplementary Fig. S1A-C**). The transcriptome of CD103$^+$ CTLs was characterized by an activation and exhaustion signature (**Supplementary Table S7**) with significant upregulation of *GZMB* (granzyme B), *HAVCR2* (T-cell immunoglobulin and mucin domain 3, TIM3), *LAG3* (lymphocyte-activation gene 3), *TNFRSF18* (glucocorticoid-induced TNFR-related protein, GITR), *KIR2DL4* (killer cell immunoglobulin-like receptor 2DL4), *TIGIT* (T-cell immunoreceptor with Ig and ITIM domain), and *CTLA4* (cytotoxic T-lymphocyte attenuator 4) in the 20-cell pools (**Fig. 1B**). CD103$^+$ CTLs expressed *GNGT2* (G protein subunit gamma transducin 2), encoding a G protein gamma family member expressed in lymph nodes and spleen that is involved in GTPase activity (**Fig. 1B**). The expression of these markers is in-line with our earlier work demonstrating that the intraepithelial CD103$^+$ T cells likely represent CTLs that have undergone activation and/or exhaustion [26,32]. By contrast, CD103$^-$ CTLs displayed a more quiescent phenotype with a high differential expression of the V-set domain–containing T-cell activation inhibitor 1 (*VTCN1*), a known suppressor of T-cell function (**Fig. 1B**). These cells differentially expressed *GAGE12H, GAGE12I,* and *GMPR2* (guanosine monophosphate reductase 2), involved in cell energy metabolism (**Fig. 1B**). Finally, CD103$^+$, but not CD103$^-$, cells were characterized by expression of genes previously associated [35] with exhausted CD8$^+$ T cells (**Fig. 1C**).

CD103$^+$ CTLs differentially express the B-cell recruiting chemokine CXCL13

In addition to the activated and exhausted gene signature, CD103$^+$ CTLs were also characterized by significantly upregulated expression of the TLS-inducing *CXCL13* (**Fig. 1B and 1D**; $p<0.0001$).

Although traditionally considered a $CD4^+$ follicular helper T-cell (TFH) gene, *CXCL13* is also expressed in subsets of $CD8^+$ TILs from hepatocellular carcinoma, melanoma, breast, and non-small cell lung cancer [36–39]. In the latter, *CXCL13* was identified in a transcriptionally unique PD-1–high ($PD\text{-}1^T$) $CD8^+$ T-cell population that predicted response to ICI therapy [36]. We, therefore, determined whether ovarian tumor-infiltrating $CD103^+$ and $PD\text{-}1^T$ $CD8^+$ populations overlapped phenotypically. PD-1 was differentially expressed in $CD103^+$ over $CD103^-$ cells on the mRNA level, although this did not reach statistical significance in the 20-cell pools (**Fig. 1B-C**). Nevertheless, at the protein level, PD-1 was expressed almost exclusively on the cell surface of $CD103^+CD8^+$ T cells (**Fig. 1E-F**), although considerable heterogeneity existed between patients with regards to PD-1 expression (**Fig. 1E**). Accordingly, analysis of the $CD103^+$ and $CD103^-$ CD8+ single-cell mRNA sequencing data revealed that *PDCD1* was heterogeneously expressed in $CD103^+$ cells but absent in $CD103^-$ cells (**Fig. 1G**). By contrast, *CXCL13* was homogenously expressed in almost all $CD103^+CD8^+$ T cells (**Fig. 1G**). In line with the above, *CXCL13* and *PDCD1* transcripts were significantly, although poorly, correlated (**Fig. 1H**). Finally, we assessed whether $CD103^+$ TILs secreted CXCL13 protein, using $CD4^+$ TILs obtained by flow cytometry-based sorting as controls. $CD103^+CD8^+$ TILs and $CD4^+$ TILs readily secreted CXCL13 upon *ex vivo* activation with anti-CD3/anti-CD28-conjugated beads or PMA/ionomycin (**Fig. 1I**).

TGFβ primes cytotoxic $CD8^+$ T cells to secrete CXCL13 *in vitro*

We next sought to define the molecular mechanism underlying production of CXCL13 by $CD103^+CD8^+$ TILs. Previously, we and others have demonstrated that induction of CD103 on $CD8^+$ T cells is dependent on concurrent T-cell receptor (TCR) and transforming growth factor beta (TGFβ) receptor 1 (TGFβR1) signaling [26,40]. TGFβ is a reported inducer of exhaustion-related genes such as PD-1 in T cells [41], which is also in-line with the transcriptional and phenotypical profile that we obtained for $CD103^+CD8^+$ TILs. Therefore, we hypothesized that TGFβ might stimulate $CD8^+$ T cells to secrete CXCL13. To investigate this, we activated peripheral blood $CD8^+$ T cells from healthy donors with anti-CD3/anti-CD28-conjugated beads in the presence or absence of recombinant TGFβ1 (rTGFβ1) and measured secretion of CXCL13. Resting $CD8^+$ T cells did not produce or secrete CXCL13 (**Fig. 2A**), nor did they express CD103 at the cell surface. Activation using anti-CD3/anti-CD28–conjugated beads induced minimal secretion of CXCL13 (**Fig. 2A**) and a minor upregulation of

CD103 (**Fig. 2B**). Secretion of CXCL13 and expression of CD103 was inhibited by co-incubation with a TGFβR1 inhibitor, suggesting autocrine TGFβ signaling was required for this induction of CXCL13 (**Fig. 2A-B**). Accordingly, activation of $CD8^+$ T cells in the presence of rTGFβ1 induced significant CXCL13 secretion (**Fig. 2A**) and expression of CD103 on the CD8 T-cell surface (**Fig. 2B**). Again, induction of CXCL13 and CD103 were inhibited by co-incubation with a TGFβR1 inhibitor (**Fig. 2A-B**). Induction of CXCL13 by TGFβ was dose-dependent and induced CXCL13 secretion at 0,1 ng/mL rTGFβ1 with a peak at 10 ng/mL rTGFβ1 (**Fig. 2C**). Because IL2 inhibits the secretion of CXCL13 in follicular helper $CD4^+$ T cells [42], we also examined whether IL2 impacted CXCL13 secretion by $CD8^+$ T cells. In contrast to $CD4^+$ T cells, induction of CXCL13 in $CD8^+$ T cells was not inhibited by IL2 (**Fig. 2D**), suggesting underlying differences in CXCL13 gene regulation and/or IL2 signaling between $CD8^+$ and $CD4^+$ cells. Based on our findings, we concluded that TGFβ was sufficient for CXCL13 induction in activated $CD8^+$ T cells.

Next, we determined whether TGFβ also modulates secretion of other chemokines. Analysis of chemokine mRNA expression in $CD103^+$ vs. $CD103^-$ TILs revealed a significant upregulation of CCL3, CCL5, and CXCL13 and a trend towards overexpression of CCL3L1, CCL4L2, CCL20, and CXCL9 in $CD103^+$ TILs (**Fig. 2E**). Subsequent analysis of 47 chemokines secreted from peripheral blood $CD8^+$ T cells revealed activation-dependent production of CCL4, CCL5, CXCL9, and CXCL10 (**Fig. 2F-G and Supplementary Fig. S2A-C**). As before, significantly higher CXCL13 was secreted upon activation of T cells in the presence of rTGFβ1 (**Fig. 2H-I**). By contrast, rTGFβ1 did not affect the induction of other chemokines (**Fig. 2I**). Taken together, our data indicated that TGFβ was a specific inducer of CXCL13 in $CD8^+$ T cells and identified a hallmark chemokine pattern for $CD103^+CD8^+$ TILs.

$CXCL13^+CD103^+$ CTLs associated with a high mutation load, B-cell infiltration, and TLSs

CXCL13 is a key driver of B-cell recruitment and TLS formation in cancer and autoimmune diseases [43–47]. As such, we speculated the $CXCL13^+CD103^+$ TIL population would be involved in recruitment of B cells and TLS formation across human tumors. We retrospectively analyzed a cohort of 125 (high-grade serous) ovarian tumors for $CD103^+$ cells and $CD20^+$ B cells using a tissue microarray. $CD103^+$ and $CD20^+$ cells were detected in most patients, with some $CD20^+$ cells forming aggregates in close proximity to $CD103^+$ cells in the tumor epithelium (**Fig. 3A**). Indeed, division of

patients by high (>26.3), intermediate (8.6-26.3), or low (<8.6) $CD103^+$ cell infiltration revealed a significant association with the number of B cells (**Fig. 3B**). Next, we assessed whether $CD103^+CD8^+$ T cells might also link neoantigen-specific T-cell responses to B cell–driven immune responses. To address this, we determined whether tumors with a high neoantigen load and concomitantly high CD103+ TIL infiltrate were enriched for B cell– and TLS-associated genes in mRNA sequencing data from The Cancer Genome Atlas (TCGA). Specifically, we analyzed uterine cancer (UC) samples stratified by neoantigen load. In brief, four distinct molecular subtypes can be distinguished in UC: microsatellite stable (MSS), microsatellite unstable (MSI), polymerase epsilon exonuclease domain mutated (*POLE*-EDM) tumors, and p53-mutant tumors. We have previously demonstrated an increased number of mutations, predicted neoantigens, and ($CD103^+$) T cells in *POLE*-EDM and MSI tumors compared to MSS tumors [25]. In-line with the above, MSS tumors mostly lacked B-cell– and TLS-related genes, whereas MSI and *POLE*-EDM tumors were enriched for these genes (**Fig. 3C**). To confirm these findings, we further analyzed an independent cohort of MSS, MSI, and *POLE*-EDM tumors from UC patients for the presence of $CD20^+$ B cells by immunohistochemistry. B cells were predominantly observed in large aggregations in the tumor and surrounding stroma (**Fig. 3D-E**). In-line with the TCGA data, only 48% (20/42) of MSS tumors were found to have B-cell aggregates, whereas 74% (28/38) of MSI and 92% (33/36) of *POLE*-EDM tumors contained B-cell aggregates (**Fig. 3D**). Quantification per tumor revealed a significant increase in the number of B-cell aggregates when comparing MSS to *POLE*-EDM and MSI to *POLE*-EDM tumors (**Fig. 3D**, $p<0.001$ and $p<0.01$, respectively). To confirm that the observed B-cell aggregates were phenotypically similar to TLSs, we performed multi-color immunofluorescence. Indeed, B-cell aggregates showed the typical characteristics of lymphoid tissues, as determined by the presence of high endothelial venules (HEVs), germinal B-cell centers, and DCs surrounded by a rim of T cells (**Fig. 3F**).

Based on the above, we speculated that $CXCL13^+CD103^+$ CTL genes would associate with TLS genes across human epithelial tumors. To assess this, we analyzed TCGA mRNA expression data of ovarian, uterine, lung, and breast cancer using the differentially expressed genes from $CXCL13^+CD103^+$ and $CXCL13^-CD103^-$ CTL cells identified by our mRNA sequencing. TLS genes correlated with $CXCL13^+CD103^+$, but not $CXCL13^-CD103^-$, CTL genes across all four tumor types

(**Fig. 4**). Taken together, our data suggested that CXCL13^{+}CD103^{+} CTLs promote migration of B cells to tumors and the formation of TLSs across tumor types.

CXCL13+CD103+CD8 cells correlate to improved survival irrespective of neoantigen burden

To assess whether CXCL13^{+}CD103^{+} CTLs were also correlated with improved survival, we analyzed clinical outcomes in two cohorts of uterine cancer patients. We focused on tumors with a low neoantigen burden because a high neoantigen load is associated with better survival. First, we analyzed TCGA endometrial cancers of the MSS subtype and correlated high *CXCL13* and CD103 (*ITGAE*) gene expression to survival. *CXCL13*^{high}*ITGAE*^{high} MSS tumors had a significantly improved survival as compared to *CXCL13*^{low}*ITGAE*^{low} MSS tumors from TCGA (**Supplementary Fig. S3A**). To confirm this survival benefit for CXCL13^{+}CD103^{+} CTLs in neoantigen low tumors, we analyzed FFPE tumor tissue of an independent cohort of mismatch repair proficient (pMMR) uterine cancers by immunohistochemistry (**Supplementary Table S8**). We were unable to detect CXCL13 protein expression in CD103^{+} CTLs, consistent with our previous finding that almost all CD103^{+} cells express CXCL13 on the mRNA level (**Fig. 1B, 1D, and 1G**), but express and secrete the protein only after re-activation (**Fig. 1I**). Therefore, we analyzed the effect of CXCL13^{+}CD103^{+} CTL infiltration on clinical outcome in this cohort by proxy, using CD103 staining. We observed a significant survival benefit for patients with mismatch repair proficient tumors infiltrated by a high number of CD103^{+} cells over tumors infiltrated by a low number of CD103^{+} cells (**Supplementary Fig. S3B**). This effect was independent of other clinical variables, as demonstrated by multivariate analysis (**Table 1**). As such, our data demonstrated that (CXCL13^{+}) CD103^{+} CTLs are associated with improved clinical outcome, independent of neoantigen burden.

Discussion

In this study we reported on the finding that TGFβ stimulates activated CD8^{+} T cells to produce CXCL13, a known inducer of TLSs [17–19]. This production of CXCL13 was paralleled by the induction of CD103 on the cell surface of CD8^{+} cells *in vitro*. CD103^{+}CD8^{+} T cells isolated directly from human tumors expressed *CXCL13* mRNA and secreted CXCL13 protein upon *ex vivo* reactivation. The presence of B cell and TLS genes was increased in mutated, CXCL13^{+}CD103^{+}CD8^{+}

T cell–enriched human tumors from TCGA, and the absolute number of B cells associated with a high load of predicted neoantigens in an independent cohort of uterine cancers and a cohort of high-grade serous ovarian cancers. Our findings shed light on the link between $CD8^+$ T-cell activation and the migration of B cells into the tumor. Our data also identified CD103 and B cells as potential biomarkers of interest for cancer immunotherapy.

CXCL13 is generally associated with DCs and TFH [42,48,49]. Nevertheless, single-cell sequencing of exhausted, tumor-infiltrating T cells of liver cancer, breast cancer, lung cancer, and melanoma does support expression of *CXCL13* in TILs [36–38]. We found that TGFβ1, a cytokine mostly associated with immune suppression [42,50–52], was essential for the induction of CXCL13. Under homeostatic conditions, TGFβ1 is abundantly present in epithelial tissue and controls the epithelial localization of resident memory immune subsets, such as the intraepithelial lymphocytes in the colon [53]. In epithelial cancers, we suggest that TGFβ1 has a similar role in promoting not only recruitment, signaling, and retention of $CD8^+$ T cells via CD103 expression [54], but also stimulating immunity via attraction of C-X-C chemokine receptor type 5 $(CXCR5)^+$ immune cells through CXCL13 signaling.

CXCL13 is the key molecular determinant of TLS formation [17–19], ectopic lymphoid structures that are thought to enable efficient local priming of T cells by DCs [9]. Hereby, the time-consuming migration of DCs and T cells to and from lymph nodes may be circumvented, augmenting local antitumor immunity. In-line with this, characteristic components of TLSs, such as HEVs and B cells, are found to be generally associated with an improved prognosis [10], and plasma B cells in the TLSs are thought to enhance antitumor responses by production and subsequent accumulation of antitumor antibodies, potentially leading to antibody-dependent cytotoxicity and opsonization [12]. Thus, TLSs may orchestrate a joint T- and B-cell response to improve antitumor immunity.

Because TLSs were more abundant in tumors with a high mutational load, we postulated that activated $CD103^+$ CTLs were involved in the migration of B cells to tumors via production of CXCL13. This is supported by our observations that mutated, $CD8^+$ T cell–rich tumors showed higher expression of *CXCL13* and *ITGAE (*CD103) and that they presented with significantly higher numbers of B cells. In accordance, a higher degree of TCR clonality within $CD8^+$ T cells correlates with a higher number of TLSs in non-small cell lung cancer [55]. These TLSs may represent an ongoing immune response that is insufficient to halt tumor progression at an early time point. It would, therefore, be of

great interest to study the induction and formation of TLSs in developing cancer lesions and to determine whether $CD8^+$ T-cell infiltration precedes TLS formation.

In-line with previous work [26,32,56], $CD103^+$ CTLs from human tumors were also characterized by an activation- and exhaustion-related gene expression signature, with differential expression of granzymes and well-known immune checkpoint molecules, such as *CTLA4*. $CD103^+$ CTLs expressed several additional immune checkpoint genes currently under clinical investigation, such as *TIM3*, *LAG3*, and *TIGIT*. This observed phenotype is concordant with a reported subset of PD-1–high ($PD\text{-}1^T$) $CD8^+$ T cells in lung cancer [36]. The $PD\text{-}1^T$ subset was transcriptionally distinct and characterized by expression of *CXCL13*. This subset also expressed higher *ITGAE*, although cell surface expression of CD103 was not examined. Nevertheless, our analysis of the gene expression profile reported for $PD\text{-}1^T$ $CD8^+$ cells [36] revealed overlapping overexpression of ~200 genes with $CD103^+CD8^+$ cells, suggesting these populations might represent the same T-cell subset. Importantly, $CXCL13^+PD\text{-}1^T$ $CD8^+$ cells are associated with response to ICI [36].

The association between $CXCL13^+PD\text{-}1^T$ $CD8^+$ cells and response to ICI is in-line with the observation that $CD103^+$ CTLs significantly expand upon treatment with nivolumab or pembrolizumab (anti–PD-1) in tumor specimens of advanced-stage metastatic melanoma patients [57]. Accordingly, a paper by Riaz et al. demonstrates that tumors from patients who responded to nivolumab treatment differentially expressed genes such as *CXCL13, CTLA4*, *TIM3*, *LAG3*, *PDCD1*, *GZMB,* and tumor necrosis factor receptor superfamily member 9 (*TNFRSF9*), all genes overexpressed in $CD103^+$ vs. $CD103^-$ CTLs [7]. Pre-treatment, but not on-treatment, *CXCL13* was differentially expressed in responders vs. non-responders in this study [7]. This may be explained by the low basal CXCL13 secretion we observed in the exhausted, $CD103^+$ CTLs freshly isolated from untreated human tumors. In their exhausted state, CTLs might accumulate mRNA encoding several key effector molecules that is translated only upon reactivation (e.g. by ICI). Consistent with this, Riaz et al. observed an increase in the number of B cell–related genes on-treatment in responding patients [7], perhaps hinting at B-cell recruitment and the formation of TLSs in these patients upon ICI-mediated release of CXCL13. This hypothesis is supported by the observed increases in serum CXCL13 and concomitant depletion of $CXCR5^+$ B cells from the circulation in patients treated with anti–CTLA-4 and/or anti–PD-1 [58]. Our data, therefore, suggest that ICIs are of particular interest for patients with a high $CXCL13^+CD103^+$ CTL infiltration pre-treatment across malignancies.

Several combination immunotherapy regimes that promote $CD8^+$ T-cell infiltration and TLS formation may also function via $CD8^+$ T cell–dependent production of CXCL13. For instance, combined therapy with anti-angiogenic and immunotherapeutic agents in mice stimulated the transformation of tumor blood vessels into intratumoral HEVs, which subsequently enhanced the infiltration and activation of $CD8^+$ T cells and the destruction of tumor cells [59,60]. These T cells formed structures around HEVs that closely resembled TLSs [59,60]. One of these studies found that induction of TLSs was dependent on both $CD8^+$ T cells and macrophages [59]. However, the exact intratumoral mechanism of action remains unclarified. Because macrophages produce TGFβ in a chronically inflamed environment [42], we hypothesize that the macrophages in these studies may have generated a TGFβ-enriched environment, thus, leading to the production of CXCL13 chemokine by activated T cells and subsequently to the formation of lymphoid structures. TLSs may, therefore, reflect an ongoing $CD8^+$ T-cell response in cancer. As such, TLSs may be used as a biomarker to predict response to ICI, and these structures may be used as a general biomarker for response to immunotherapy because TLS were found to identify pancreatic cancer patients who responded to therapeutic vaccination [61].

Taken together, we demonstrated that TGFβ1 induces co-expression of CXCL13 and CD103 in $CD8^+$ T cells, potentially linking $CD8^+$ T-cell activation to B cell migration and TLS formation. Our findings provide a perspective on how (neo)antigens could promote the formation of TLSs in human tumors. Accordingly, $CD103^+$ cells and B cells should be considered as a potential predictive or response biomarker for immune checkpoint inhibitor therapy.

Acknowledgements

The authors would like to thank Henk Moes, Geert Mesander, Johan Teunis, Joan Vos, and Niels Kouprie for their technical assistance. This work was supported by Dutch Cancer Society/Alpe d'Huzes grant UMCG 2014−6719 to MB, Dutch Cancer Society Young Investigator Grant 10418 to TB, Jan Kornelis de Cock Stichting grants to FLK, KLB, FAE and HHW, Nijbakker-Morra Stichting and Studiefonds Ketel1 grants to HHW, the Oxford NIHR Comprehensive Biomedical Research Centre, core funding to the Wellcome Trust Centre for Human Genetics from the Wellcome Trust (090532/Z/09/Z), a Wellcome Trust Clinical Training Fellowship to MG and a Health

Foundation/Academy of Medical Sciences Clinician Scientist Fellowship award to DNC. The views expressed are those of the authors and not necessarily those of the NHS, the NIHR, the Department of Health, or the Wellcome Trust.

References

1. Ansell SM, Lesokhin AM, Borrello I, Halwani A, Scott EC, Gutierrez M, Schuster SJ, Millenson MM, Cattry D, Freeman GJ, Rodig SJ, Chapuy B, Ligon AH, Zhu L, et al. PD-1 Blockade with Nivolumab in Relapsed or Refractory Hodgkin's Lymphoma. N Engl J Med [Internet]. 2015;372:311–9. Available from: http://www.nejm.org/doi/10.1056/NEJMoa1411087
2. Hamid O, Robert C, Daud A, Hodi FS, Hwu W-J, Kefford R, Wolchok JD, Hersey P, Joseph RW, Weber JS, Dronca R, Gangadhar TC, Patnaik A, Zarour H, et al. Safety and Tumor Responses with Lambrolizumab (Anti–PD-1) in Melanoma. N Engl J Med [Internet]. 2013;369:134–44. Available from: http://www.nejm.org/doi/10.1056/NEJMoa1305133
3. Borghaei H, Paz-Ares L, Horn L, Spigel DR, Steins M, Ready NE, Chow LQ, Vokes EE, Felip E, Holgado E, Barlesi F, Kohlhäufl M, Arrieta O, Burgio MA, et al. Nivolumab versus Docetaxel in Advanced Nonsquamous Non–Small-Cell Lung Cancer. N Engl J Med [Internet]. 2015;373:1627–39. Available from: http://www.nejm.org/doi/10.1056/NEJMoa1507643
4. Pardoll DM. The blockade of immune checkpoints in cancer immunotherapy. Nat Rev Cancer. 2012;12:252–64.
5. Snyder A, Makarov V, Merghoub T, Yuan J, Zaretsky JM, Desrichard A, Walsh LA, Postow MA, Wong P, Ho TS, Hollmann TJ, Bruggeman C, Kannan K, Li Y, et al. Genetic Basis for Clinical Response to CTLA-4 Blockade in Melanoma. N Engl J Med [Internet]. 2014;371:2189–99. Available from: http://www.nejm.org/doi/10.1056/NEJMoa1406498
6. Rizvi NA, Hellmann MD, Snyder A, Kvistborg P, Makarov V, Havel JJ, Lee W, Yuan J, Wong P, Ho TS, Miller ML, Rekhtman N, Moreira AL, Ibrahim F, et al. Mutational landscape determines sensitivity to PD-1 blockade in non – small cell lung cancer. 2016;348:124–9.
7. Riaz N, Havel JJ, Makarov V, Desrichard A, Urba WJ, Sims JS, Hodi FS, Martín-Algarra S, Mandal R, Sharfman WH, Bhatia S, Hwu WJ, Gajewski TF, Slingluff CL, et al. Tumor and Microenvironment Evolution during Immunotherapy with Nivolumab. Cell. 2017;171:934–949.e15.
8. Dieu-Nosjean MC, Goc J, Giraldo NA, Saut??s-Fridman C, Fridman WH. Tertiary lymphoid structures in cancer and beyond. Trends Immunol. 2014;35:571–80.
9. Dieu-Nosjean MC, Giraldo NA, Kaplon H, Germain C, Fridman WH, Sautès-Fridman C. Tertiary lymphoid structures, drivers of the anti-tumor responses in human cancers. Immunol

Rev. 2016;271:260–75.

10. Sautès-Fridman C, Lawand M, Giraldo NA, Kaplon H, Germain C, Fridman WH, Dieu-Nosjean MC. Tertiary lymphoid structures in cancers: Prognostic value, regulation, and manipulation for therapeutic intervention. Front Immunol. 2016;7:1–11.
11. Giraldo NA, Becht E, Pagès F, Skliris G, Verkarre V, Vano Y, Mejean A, Saint-Aubert N, Lacroix L, Natario I, Lupo A, Alifano M, Damotte D, Cazes A, et al. Orchestration and prognostic significance of immune checkpoints in the microenvironment of primary and metastatic renal cell cancer. Clin Cancer Res. 2015;21:3031–40.
12. Kroeger DR, Milne K, Nelson BH. Tumor-infiltrating plasma cells are associated with tertiary lymphoid structures, cytolytic T-cell responses, and superior prognosis in ovarian cancer. Clin Cancer Res. 2016;22:3005–15.
13. Pimenta EM, Barnes BJ. Role of tertiary lymphoid structures (TLS) in anti-tumor immunity: Potential tumor-induced cytokines/chemokines that regulate TLS formation in epithelial-derived cancers. Cancers (Basel). 2014;6:969–97.
14. Ansel KM, Harris RBS, Cyster JG. CXCL13 is required for B1 cell homing, natural antibody production, and body cavity immunity. Immunity. 2002;16:67–76.
15. Van De Pavert SA, Olivier BJ, Goverse G, Vondenhoff MF, Greuter M, Beke P, Kusser K, Höpken UE, Lipp M, Niederreither K, Blomhoff R, Sitnik K, Agace WW, Randall TD, et al. Chemokine cxcl13 is essential for lymph node initiation and is induced by retinoic acid and neuronal stimulation. Nat Immunol [Internet]. Nature Publishing Group; 2009;10:1193–9. Available from: http://dx.doi.org/10.1038/ni.1789
16. Ansel KM, Ngo VN, Hyman PL, Luther SA, Förster R, Sedgwlck JD, Browning JL, Upp M, Cyster JG. A chemokine-driven positive feedback loop organizes lymphoid follicles. Nature. 2000;406:309–14.
17. Luther SA, Ansel KM, Cyster JG. Overlapping Roles of CXCL13, Interleukin 7 Receptor α, and CCR7 Ligands in Lymph Node Development. J Exp Med [Internet]. 2003;197:1191–8. Available from: http://www.jem.org/lookup/doi/10.1084/jem.20021294
18. Luther SA, Lopez T, Bai W, Hanahan D, Cyster JG. BLC expression in pancreatic islets causes B cell recruitment and lymphotoxin-dependent lymphoid neogenesis. Immunity. 2000;12:471–81.

19. Gräbner R, Lötzer K, Döpping S, Hildner M, Radke D, Beer M, Spanbroek R, Lippert B, Reardon CA, Getz GS, Fu Y-X, Hehlgans T, Mebius RE, van der Wall M, et al. Lymphotoxin β receptor signaling promotes tertiary lymphoid organogenesis in the aorta adventitia of aged *ApoE* $^{-/-}$ mice. J Exp Med [Internet]. 2009;206:233–48. Available from: http://www.jem.org/lookup/doi/10.1084/jem.20080752

20. Thommen DS, Koelzer VH, Herzig P, Roller A, Trefny M, Dimeloe S. Europe PMC Funders Group Europe PMC Funders Author Manuscripts A transcriptionally and functionally distinct PD-1 + CD8 + T cell pool with predictive potential in non-small cell lung cancer treated with PD-1 blockade. 2018;24:994–1004.

21. Riaz N, Havel JJ, Makarov V, Desrichard A, Urba WJ, Sims JS, Hodi FS, Martín-Algarra S, Mandal R, Sharfman WH, Bhatia S, Hwu WJ, Gajewski TF, Slingluff CL, et al. Tumor and Microenvironment Evolution during Immunotherapy with Nivolumab. Cell. 2017;

22. Eggink FA, Van Gool IC, Leary A, Pollock PM, Crosbie EJ, Mileshkin L, Jordanova ES, Adam J, Freeman-Mills L, Church DN, Creutzberg CL, De Bruyn M, Nijman HW, Bosse T. Immunological profiling of molecularly classified high-risk endometrial cancers identifies POLE-mutant and microsatellite unstable carcinomas as candidates for checkpoint inhibition. Oncoimmunology. Taylor & Francis; 2017;6.

23. Nout RA, Bosse T, Creutzberg CL, Jürgenliemk-Schulz IM, Jobsen JJ, Lutgens LCHW, Van Der Steen-Banasik EM, Van Eijk R, Ter Haar NT, Smit VTHBM. Improved risk assessment of endometrial cancer by combined analysis of MSI, PI3K-AKT, Wnt/β-catenin and P53 pathway activation. Gynecol Oncol. 2012. page 466–73.

24. Creutzberg CL, van Putten WL, Koper PC, Lybeert ML, Jobsen JJ, Wárlám-Rodenhuis CC, De Winter KA, Lutgens LC, van den Bergh AC, van de Steen-Banasik E, Beerman H, van Lent M. Surgery and postoperative radiotherapy versus surgery alone for patients with stage-1 endometrial carcinoma: multicentre randomised trial. PORTEC Study Group. Post Operative Radiation Therapy in Endometrial Carcinoma. Lancet [Internet]. 2000;355:1404–11. Available from: http://www.ncbi.nlm.nih.gov/pubmed/10791524

25. Van Gool IC, Eggink FA, Freeman-Mills L, Stelloo E, Marchi E, De Bruyn M, Palles C, Nout RA, De Kroon CD, Osse EM, Klenerman P, Creutzberg CL, Tomlinson IPM, Smit VTHBM, et al. POLE proofreading mutations elicit an antitumor immune response in endometrial cancer.

Clin Cancer Res. 2015;21:3347–55.

26. Komdeur FL, Wouters MCA, Workel HH, Tijans AM, Leffers N, Helfrich W, Samplonius DF, Bremer E, Bruyn M De. CD103 + intraepithelial T cells in high-grade serous ovarian cancer are phenotypically diverse TCRαβ + CD8αβ + T cells that can be targeted for cancer immunotherapy. 2016;7.

27. Rayner E, van Gool IC, Palles C, Kearsey SE, Bosse T, Tomlinson I, Church DN. A panoply of errors: polymerase proofreading domain mutations in cancer. Nat Rev Cancer [Internet]. 2016;16:71–81. Available from: http://www.nature.com/doifinder/10.1038/nrc.2015.12%5Cnhttp://www.ncbi.nlm.nih.gov/pubmed/26822575

28. Bindea G, Mlecnik B, Tosolini M, Kirilovsky A, Waldner M, Obenauf AC, Angell H, Fredriksen T, Lafontaine L, Berger A, Bruneval P, Fridman W, Becker C, Pagès F, et al. Spatiotemporal dynamics of intratumoral immune cells reveal the immune landscape in human cancer. Immunity. 2013;39:782–95.

29. Workel HH, Komdeur FL, Wouters MCA, Plat A, Klip HG, Eggink FA, Wisman GBA, Arts HJG, Oonk MHM, Mourits MJE, Yigit R, Versluis M, Duiker EW, Hollema H, et al. CD103 defines intraepithelial CD8+ PD1+ tumour-infiltrating lymphocytes of prognostic significance in endometrial adenocarcinoma. Eur J Cancer. 2016;60:1–11.

30. Picelli S, Faridani OR, Björklund ÅK, Winberg G, Sagasser S, Sandberg R. Full-length RNA-seq from single cells using Smart-seq2. Nat Protoc. 2014;9:171–81.

31. Gilles Carpentier and Emilie Henault, Protein Array Analyzer for ImageJ. Proceedings of the ImageJ User and Developer Conference, Centre de Recherche Public Henri Tudor, ed., (ISBN 2-919941- 11-9), pp. 238-240, 2010.

32. Workel HH, Komdeur FL, Wouters MCA, Plat A, Klip HG, Eggink FA, Wisman GBA, Arts HJG, Oonk MHM, Mourits MJE, Yigit R, Versluis M, Duiker EW, Hollema H, et al. CD103 defines intraepithelial CD8+ PD1+ tumour-infiltrating lymphocytes of prognostic significance in endometrial adenocarcinoma. Eur J Cancer [Internet]. Elsevier Ltd; 2016;60:1–11. Available from: http://dx.doi.org/10.1016/j.ejca.2016.02.026

33. Komdeur FL, Prins TM, van de Wall S, Plat A, Wisman GBA, Hollema H, Daemen T, Church DN, de Bruyn M, Nijman HW. CD103+ tumor-infiltrating lymphocytes are tumor-reactive

intraepithelial CD8+ T cells associated with prognostic benefit and therapy response in cervical cancer. Oncoimmunology [Internet]. Taylor & Francis; 2017;6:1–14. Available from: https://doi.org/10.1080/2162402X.2017.1338230

34. Djenidi F, Adam J, Goubar A, Durgeau A, Meurice G, de Montpréville V, Validire P, Besse B, Mami-Chouaib F. CD8 $^{+}$ CD103 $^{+}$ Tumor–Infiltrating Lymphocytes Are Tumor-Specific Tissue-Resident Memory T Cells and a Prognostic Factor for Survival in Lung Cancer Patients. J Immunol [Internet]. 2015;194:3475–86. Available from: http://www.jimmunol.org/lookup/doi/10.4049/jimmunol.1402711

35. Guo X, Zhang Y, Zheng L, Zheng C, Song J, Zhang Q, Kang B, Liu Z, Jin L, Xing R, Gao R, Zhang L, Dong M, Hu X, et al. Global characterization of T cells in non-small-cell lung cancer by single-cell sequencing. Nat Med. 2018;

36. Thommen DD, Koelzer V, Herzig P, Roller A, Trefny M, Kiialainen A, Hanhart J, Schill C, Hess C, Savic Prince S, Wiese M, Lardinois D, Ho P, Klein C, et al. A transcriptionally and functionally distinct PD-1 + CD8 + T cell pool with predictive potential in non-small cell lung cancer treated with PD-1 blockade. Nat Med [Internet]. Springer US; 2018; Available from: http://dx.doi.org/10.1038/s41591-018-0057-z

37. Zheng C, Zheng L, Yoo JK, Guo H, Zhang Y, Guo X, Kang B, Hu R, Huang JY, Zhang Q, Liu Z, Dong M, Hu X, Ouyang W, et al. Landscape of Infiltrating T Cells in Liver Cancer Revealed by Single-Cell Sequencing. Cell [Internet]. Elsevier; 2017;169:1342–1356.e16. Available from: http://dx.doi.org/10.1016/j.cell.2017.05.035

38. Tirosh I, Izar B, Prakadan SM, Ii MHW, Treacy D, Trombetta JJ, Rotem A, Rodman C, Lian C, Murphy G, Fallahi-sichani M, Dutton-regester K, Lin J, Kazer SW, et al. Dissecting the multicellular exosystem of metastatic melanoma by single-cell RNA-seq. Science (80-). 2016;352:189–96.

39. Gu-Trantien C, Migliori E, Buisseret L, De Wind A, Brohée S, Garaud S, Noël G, Dang L, Lodewyckx J-N, Naveaux C, Duvillier H, Goriely S, Larsimont D, Willard-Gallo K. CXCL13-producing T FH cells link immune suppression and adaptive memory in human breast cancer. JCI Insight [Internet]. 2017;2:1–17. Available from: https://doi.org/10.1172/jci.insight.91487:e91487.%5Cnhttps://

40. Mokrani M, Klibi J, Bluteau D, Bismuth G, Mami-Chouaib F. Smad and NFAT Pathways

Cooperate To Induce CD103 Expression in Human CD8 T Lymphocytes. J Immunol [Internet]. 2014;192:2471–9. Available from: http://www.jimmunol.org/cgi/doi/10.4049/jimmunol.1302192

41. Park B V., Freeman ZT, Ghasemzadeh A, Chattergoon MA, Rutebemberwa A, Steigner J, Winter ME, Huynh T V., Sebald SM, Lee SJ, Pan F, Pardoll DM, Cox AL. TGFβ1-mediated SMAD3 enhances PD-1 expression on antigen-specific T cells in cancer. Cancer Discov. 2016;6:1366–81.

42. Kobayashi S, Watanabe T, Suzuki R, Furu M, Ito H, Ito J, Matsuda S, Yoshitomi H. TGF-β induces the differentiation of human CXCL13-producing CD4+ T cells. Eur J Immunol. 2016;46:360–71.

43. Amft N, Curnow SJ, Scheel-Toellner D, Devadas A, Oates J, Crocker J, Hamburger J, Ainsworth J, Mathews J, Salmon M, Bowman SJ, Buckley CD. Ectopic expression of the B cell-attracting chemokine BCA-1 (CXCL13) on endothelial cells and within lymphoid follicles contributes to the establishment of germinal center-like structures in Sjögren's syndrome. Arthritis Rheum. 2001;44:2633–41.

44. Steinmetz OM, Panzer U, Kneissler U, Harendza S, Lipp M, Helmchen U, Stahl RAK. BCA-1/CXCL13 expression is associated with CXCR5-positive B-cell cluster formation in acute renal transplant rejection. Kidney Int. 2005;67:1616–21.

45. Henry RA, Kendall PL. CXCL13 Blockade Disrupts B Lymphocyte Organization in Tertiary Lymphoid Structures without Altering B Cell Receptor Bias or Preventing Diabetes in Nonobese Diabetic Mice. J Immunol [Internet]. 2010;185:1460–5. Available from: http://www.jimmunol.org/cgi/doi/10.4049/jimmunol.0903710

46. Marraco SF, Neubert N, Verdeil G, Speiser D, Vergassola M, Altan-Bonnet G, Noël G, Chi VLD, Lodewyckx J-N, Naveaux C, Duvillier H, Goriely S, Larsimont D, Willard-Gallo K. CXCL13-producing TFH cells link immune suppression and adaptive memory in human breast cancer. Front Immunol [Internet]. 2017;6. Available from: https://insight.jci.org/articles/view/91487

47. Ansel KM, Ngo VN, Hyman PL, Luther SA, Förster R, Sedgwlck JD, Browning JL, Upp M, Cyster JG. A chemokine-driven positive feedback loop organizes lymphoid follicles. Nature. 2000;

48. Rasheed A-U, Rahn H-P, Sallusto F, Lipp M, Müller G. Follicular B helper T cell activity is

confined to CXCR5hiICOShi CD4 T cells and is independent of CD57 expression. Eur J Immunol [Internet]. 2006;36:1892–903. Available from: http://doi.wiley.com/10.1002/eji.200636136

49. Vissers JLM, Hartgers FC, Lindhout E, Figdor CG, Adema GJ. BLC (CXCL13) is expressed by different dendritic cell subsets in vitro and in vivo. Eur J Immunol. 2001;31:1544–9.

50. Wrzesinski SH, Wan YY, Flavell RA. Transforming growth factor-β and the immune response: Implications for anticancer therapy. Clin Cancer Res. 2007;13:5262–70.

51. Blobe G, Schiemann WP, Lodish HF. Role of transforming growth factor beta in human disease. N Engl J Med. 2000;342:1350–8.

52. Johnston CJC, Smyth DJ, Dresser DW, Maizels RM. TGF-β in tolerance, development and regulation of immunity. Cell Immunol [Internet]. Elsevier Inc.; 2015;299:14–22. Available from: http://dx.doi.org/10.1016/j.cellimm.2015.10.006

53. Konkel JE, Maruyama T, Carpenter AC, Xiong Y, Zamarron BF, Hall BE, Kulkarni AB, Zhang P, Bosselut R, Chen W. Control of the development of CD8αα+ intestinal intraepithelial lymphocytes by TGF-β. Nat Immunol. Nature Publishing Group; 2011;12:312–20.

54. Boutet M, Gauthier L, Leclerc M, Gros G, De Montpreville V, Theret N, Donnadieu E, Mami-Chouaib F. TGFβ signaling intersects with CD103 integrin signaling to promote T-Lymphocyte accumulation and antitumor activity in the lung tumor microenvironment. Cancer Res. 2016;76:1757–69.

55. Zhu W, Germain C, Liu Z, Sebastian Y, Devi P, Knockaert S, Brohawn P, Lehmann K, Damotte D, Validire P, Yao Y, Valge-Archer V, Hammond SA, Dieu-Nosjean M-C, et al. A high density of tertiary lymphoid structure B cells in lung tumors is associated with increased CD4 $^{+}$ T cell receptor repertoire clonality. Oncoimmunology [Internet]. 2015;4:e1051922. Available from: http://www.tandfonline.com/doi/full/10.1080/2162402X.2015.1051922

56. Ganesan A-P, Clarke J, Wood O, Garrido-Martin EM, Chee SJ, Mellows T, Samaniego-Castruita D, Singh D, Seumois G, Alzetani A, Woo E, Friedmann PS, King E V, Thomas GJ, et al. Tissue-resident memory features are linked to the magnitude of cytotoxic T cell responses in human lung cancer. Nat Immunol [Internet]. 2017;18:940–50. Available from: http://www.nature.com/doifinder/10.1038/ni.3775

57. Edwards J, Wilmott JS, Madore J, Nur Gide T, Quek C, Tasker A, Ferguson A, Chen J,

Hewavisenti R, Hersey P, Gebhardt T, Weninger W, Britton WJ, Saw RPM, et al. CD103+ tumor-resident CD8+ T cells are associated with improved survival in immunotherapy naive melanoma patients and expand significantly during anti-PD-1 treatment. Clin Cancer Res. 2018;

58. Das R, Bar N, Ferreira M, Newman AM, Zhang L, Bailur JK, Bacchiocchi A, Kluger H, Wei W, Halaban R, Sznol M, Dhodapkar M V, Dhodapkar KM. Early B cell changes predict autoimmunity following combination immune checkpoint blockade. J Clin Invest [Internet]. 2018;128:2–7. Available from: https://www.jci.org/articles/view/96798%0Ahttp://www.ncbi.nlm.nih.gov/pubmed/29309048

59. Johansson-Percival A, He B, Li ZJ, Kjellén A, Russell K, Li J, Larma I, Ganss R. De novo induction of intratumoral lymphoid structures and vessel normalization enhances immunotherapy in resistant tumors. Nat Immunol. 2017;18:1207–17.

60. Allen E, Jabouille A, Rivera LB, Lodewijckx I, Missiaen R, Steri V, Feyen K, Tawney J, Hanahan D, Michael IP, Bergers G. Combined antiangiogenic and anti–PD-L1 therapy stimulates tumor immunity through HEV formation. Sci Transl Med [Internet]. 2017;9:eaak9679. Available from: http://stm.sciencemag.org/lookup/doi/10.1126/scitranslmed.aak9679

61. Lutz ER, Wu AA, Bigelow E, Sharma R, Mo G, Soares K, Solt S, Dorman A, Wamwea A, Yager A, Laheru D, Wolfgang CL, Wang J, Hruban RH, et al. Immunotherapy Converts Nonimmunogenic Pancreatic Tumors into Immunogenic Foci of Immune Regulation. Cancer Immunol Res [Internet]. 2014;2:616–31. Available from: http://cancerimmunolres.aacrjournals.org/cgi/doi/10.1158/2326-6066.CIR-14-0027

Table 1. Cox regression survival analysis

Disease-specific survival - n=189

	Univariate				Multivariate			
	HR	*95% CI*		*p-value*	*HR*	*95% CI*		*p-value*
Age of diagnosis (cont)	1.022	0.989	1.056	0.197				
Grade of differentiation								
Good/moderate	ref	ref	ref	ref	ref	ref	ref	ref
Poor/undifferentiated	4.934	2.307	10.550	**<0.0001**	2.694	1.192	6.091	**0.017**
FIGO stage								
I	ref	ref	ref	ref	ref	ref	ref	ref
II	1.425	0.261	7.780	0.683	1.016	0.184	5.617	0.985
III	8.117	2.646	24.906	**<0.0001**	4.403	1.349	14.371	**0.014**
IV	22.707	7.218	71.432	**<0.0001**	15.697	4.762	51.735	**<0.0001**
Myometrial invasion								
No	ref	ref	ref	ref				
Yes	3.425	1.568	7.480	**0.002**				
LVSI								
No	ref	ref	ref	ref				
Yes	5.617	2.650	11.907	**<0.0001**				
Lymph node metastasis								
No	ref	ref	ref	ref				
Yes	4.620	1.911	11.171	**0.001**				
No sampling	0.775	0.299	2.011	0.601				
CD103								
Low	ref	ref	ref	ref	ref	ref	ref	ref
High	0.249	0.107	0.581	**0.001**	0.273	0.114	0.652	**0.003**

FIGO - International Federation of Gynecology and Obstetrics

CD103 - low is lower than or equal to median expression; high is higher than median expression

ref - reference

Figure legends

Figure 1. CD103+ CD8+ TILs display a distinct phenotype and gene signature characterized by exhaustion genes and CXCL13 expression.

A, Gating strategy of $CD103^+$ and $CD103^-$ $CD8^+$ T cells according to TCRαβ, CD3, CD56, CD4, CD8α, CD8β, and CD103 expression. One exemplary ovarian tumor is depicted. **B,** Volcano plot of up- or downregulated genes in $CD103^+$ and $CD103^-$ TILs as determined by RNA sequencing, annotated by a set of exhaustion and chemokine related genes. Significance was determined as Benjamini-Hochberg FDR <0.01 and log2 fold-change >1. **C,D,** Expression of exhaustion-related genes **(C)** *PDCD1* and *LAYN* and **(D)** chemokine *CXCL13* in the $CD103^+$ and $CD103^-$ subsets (n=20). The lines indicate median values+/- IQR. **E,** Cell surface expression of CD103 and PD-1 in gated $CD8^+$ TILs from exemplary ovarian tumor digests (n=3) determined by flow cytometry. The red line represents threshold for PD-1 positivity based on isotype control. **F**, Cell surface expression of PD-1 on $CD103^+$ and $CD103^-$ gated $CD8^+$ TIL subsets determined by flow cytometry (n=8). Graphs indicate median and IQR. **G**, Expression of *PDCD1* and *CXCL13* in single $CD103^-$ (n=12) and $CD103^+$ TILs (n=12). Graphs indicate median and IQR. Significance in (**F-G**) was determined as Mann-Whitney U test **P*<0.05, ***P*<0.01. **H**, Correlation of *PDCD1* and *CXCL13* expression in $CD103^+$ TILs (n=24). **I,** Secretion of CXCL13 by $CD103^+$ TILs and control $CD4^+$ TILs after stimulation overnight at 37°C using anti-CD3/CD28 T-cell activation beads (2 µL dynabeads per $1x10^5$ cells) or PMA/ionomycin (500x dilution according to manufacturer's instructions), determined by ELISA Mean plus S.E.M. of TILs from ovarian tumors (n=3) are depicted. Significance was determined by Kruskal-Wallis comparison with a post-hoc Dunn's test. **P*<0.05; ns, not significant.

Figure 2. TGF-β-dependent induction of CXCL13 in CD8+ T cells and CD103+ TIL chemokine profile.

A, Secretion of CXCL13 by sorted peripheral blood $CD8^+$ T cells after stimulation for 7 days using anti-CD3/CD28 T cell activation beads (2 µL per $1x10^5$ cells), recombinant TGFβ1 (100 ng/mL) and/or TGFβ1 receptor inhibitor SB431542 (10 µM), determined by ELISA. Depicted are mean plus S.E.M. of CD8+ T cells from 4 donors. Significance was determine using Kruskal-Wallis comparison with a post-hoc Dunn's test. **P*<0.05. **B,** Cell surface expression of CD103 on sorted $CD8^+$ T cells after stimulation using anti-CD3/CD28 T cell activation beads, recombinant TGFβ1 and/or TGFβ1 receptor

inhibitor SB431542 as described for **(A)**. One exemplary donor is depicted. **C,** Secretion of CXCL13 as determined by ELISA of $CD8^+$ T cells after stimulation using anti-CD3/CD28 T cell activation beads as described for **(A)** and/or varying concentrations of recombinant TGFβ1 as depicted on the x-axis. Mean plus S.D. from 3 donors is depicted. Significance was determined by a two-way ANOVA followed by a post-hoc Bonferroni test. **P*<0.05; *****P*<0.0001. **D**, Secretion of CXCL13 by sorted peripheral blood $CD8^+$ T cells after stimulation using anti-CD3/CD28 T cell activation beads, recombinant TGFβ1 and/or TGF-β1 receptor inhibitor SB431542 (as described for **(A)**) in the presence of IL2 (100 IU/mL), determined by ELISA. Depicted are mean plus S.E.M. of $CD8^+$ T cells from 4 donors. Significance was determine using Kruskal-Wallis comparison with a post-hoc Dunn's test. **P*<0.05. **E,** Up- or downregulated chemokines between $CD103^+$ and $CD103^-$ TILs determined by differential expression of RNA sequencing of 20-cell pools (n=20). Dashed red line indicates ≥2-fold change; dashed blue line indicates ≤0.5-fold change. Error bars indicate fold-change standard error. Significance was determined using Benjamini-Hochberg FDR. **F,** Secretion of chemokines by $CD8^+$ T cells after 7 days stimulation using anti-CD3/CD28 T cell activation beads (2 µL per $1x10^5$ cells) determined by a chemokine array kit. n=3. Shown are Log_2 fold changes of the mean compared to resting unstimulated $CD8^+$ T cells. Dashed red line indicates ≥2-fold change; dashed blue line indicates ≤ 0.5-fold change. Error bars indicate S.E.M. **G.** Exemplary chemokine array data from anti-CD3/CD28-activated $CD8^+$ T cells of one donor depicting chemokines with ≥2-fold and ≤0.5-fold change compared to resting $CD8^+$ T cells from panel (**F**). **H,I,** Secretion of chemokines by $CD8^+$ T cells after stimulation using anti-CD3/CD28 T cell activation beads and recombinant TGFβ1 (n=4). Shown are Log_2 fold changes of the mean compared to **(H)** resting unstimulated $CD8^+$ T cells or to **(I)** anti-CD3/CD28-activated $CD8^+$ T cells. Dashed red line indicates ≥2-fold change; dashed blue line indicates ≤0.5-fold change. Error bars indicate S.E.M. Significance in (**F-I**) was determine using Kruskal-Wallis comparison with a post-hoc Dunn's test. **P*<0.05 ***P*<0.01 *****P*<0.0001.

Figure 3. B cells, tertiary lymphoid structures, and correlation to $CD103^+CD8^+$ T cells in human tumors.

A,B Immunohistochemical analysis of $CD103^+$ and $CD20^+$ cells in ovarian cancer. **(A)** Exemplary image of a $CD20^+$ aggregate in close proximity to $CD103^+$ cells in the tumor epithelium and **(B)** B-cell infiltration in CD103-low, CD103-intermediate, and CD103-high tumors stratified by tertile (n=125).

Significance was determine using Kruskal-Wallis comparison with a post-hoc Dunn's test. **P*<0.05 ****P*<0.001. **C,** Gene expression of B cell–, tertiary lymphoid structure–, cytotoxic T cell–, $CD8^+$ T cell–, and $CD4^+$ follicular helper T cell–associated genes in TCGA data of uterine cancer (UCEC, n=546). Tumors were ranked according to molecular subtype and then by CD20 expression. **D,E,** Prevalence and number of B-cell aggregates (**D**) in MSS, MSI, and *POLE*-EDM uterine cancers. **(E)** One exemplary image of each subtype is depicted. Significance was determine using Kruskal-Wallis comparison with a post-hoc Dunn's test. ***P*<0.01 ****P*<0.001. **F,** Immunofluorescent analysis of CD20 aggregates in uterine cancer. CD20 aggregate expression of characteristic TLS markers CD11c, PNAD, CD20, CD38, CD79A, CD138, CD3, and CD8, one exemplary image is depicted.

Figure 4. $CXCL13^+CD103^+$ TIL genes correlate with TLS-associated genes across cancer types. Spearman correlation of genes associated with TLS, $CD103^+CD8^+$ cells, and $CD103^-CD8^+$ cells in ovarian (n=307), uterine (n=546), lung (n=517) and breast (n=1100) cancer. Correlation plots depict relative correlation of $\log_2$+1 transformed mRNA sequencing data from TCGA.

Author Manuscript Published OnlineFirst on March 14, 2019; DOI: 10.1158/2326-6066.CIR-18-0517
Author manuscripts have been peer reviewed and accepted for publication but have not yet been edited.

Figure 1

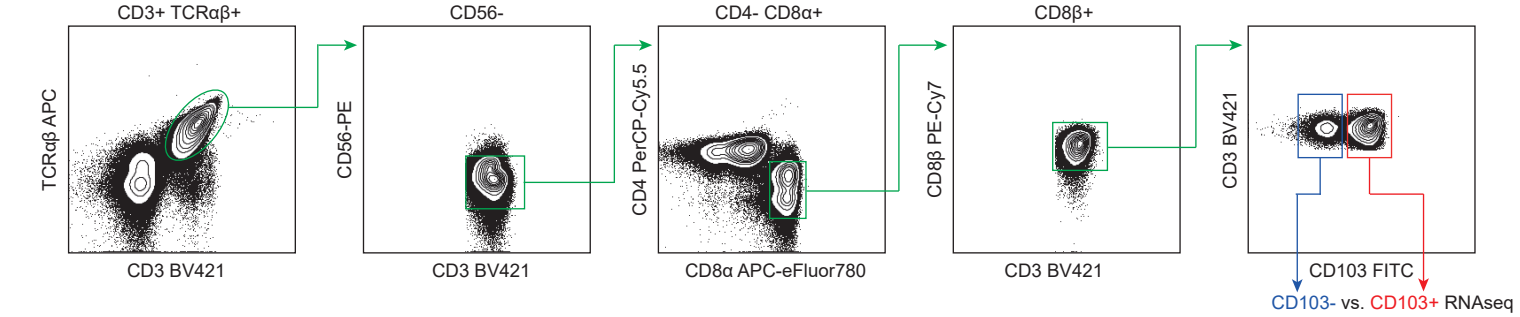

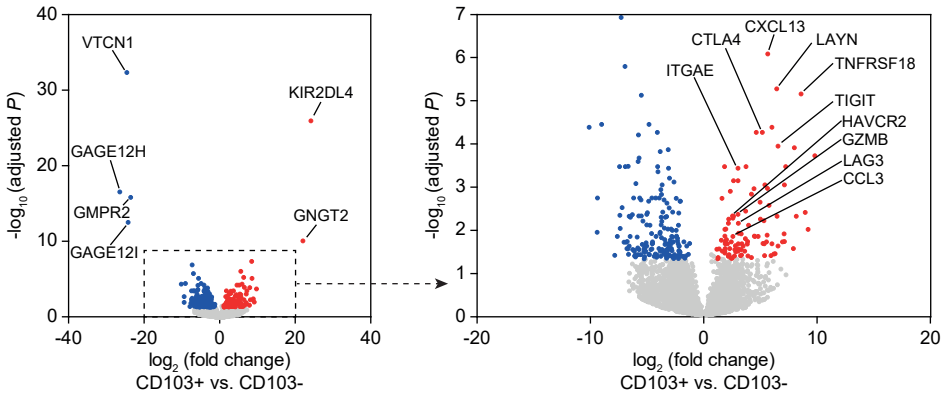

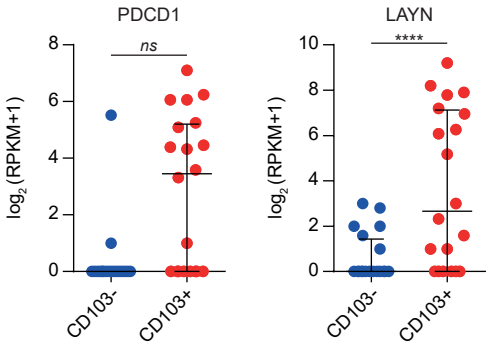

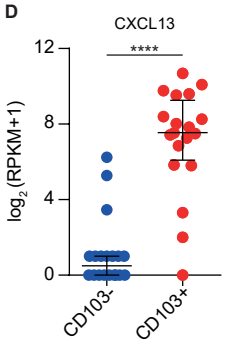

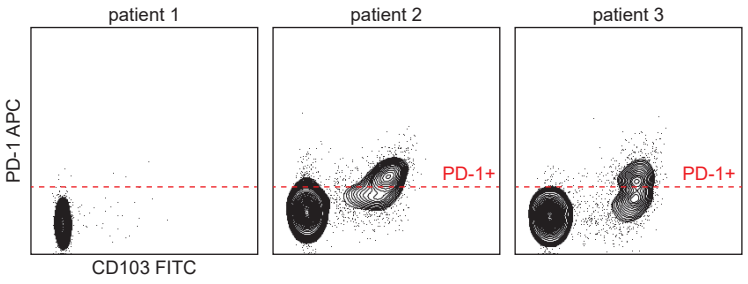

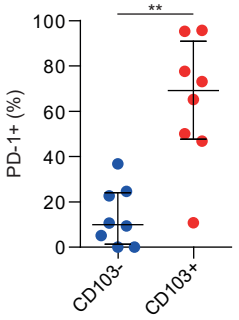

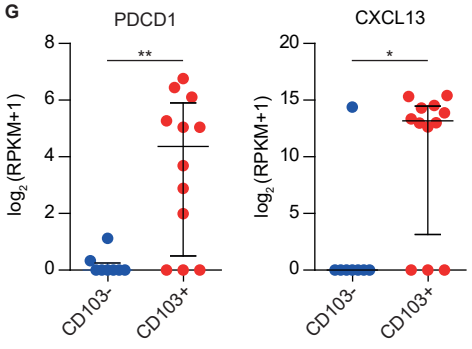

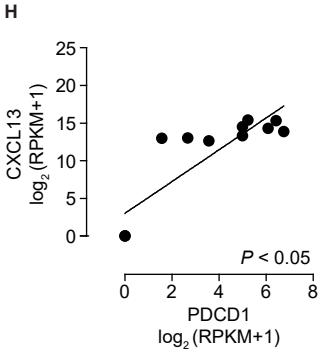

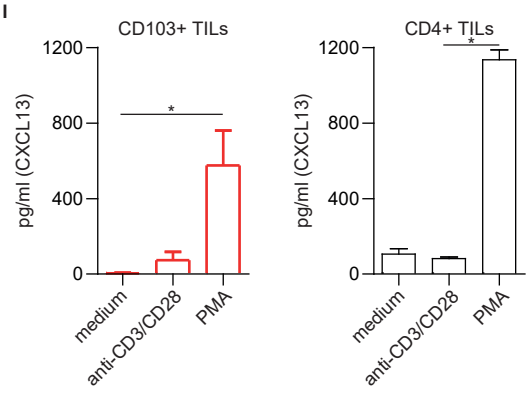

Author Manuscript Published OnlineFirst on March 14, 2019; DOI: 10.1158/2326-6066.CIR-18-0517
Author manuscripts have been peer reviewed and accepted for publication but have not yet been edited.

Figure 2

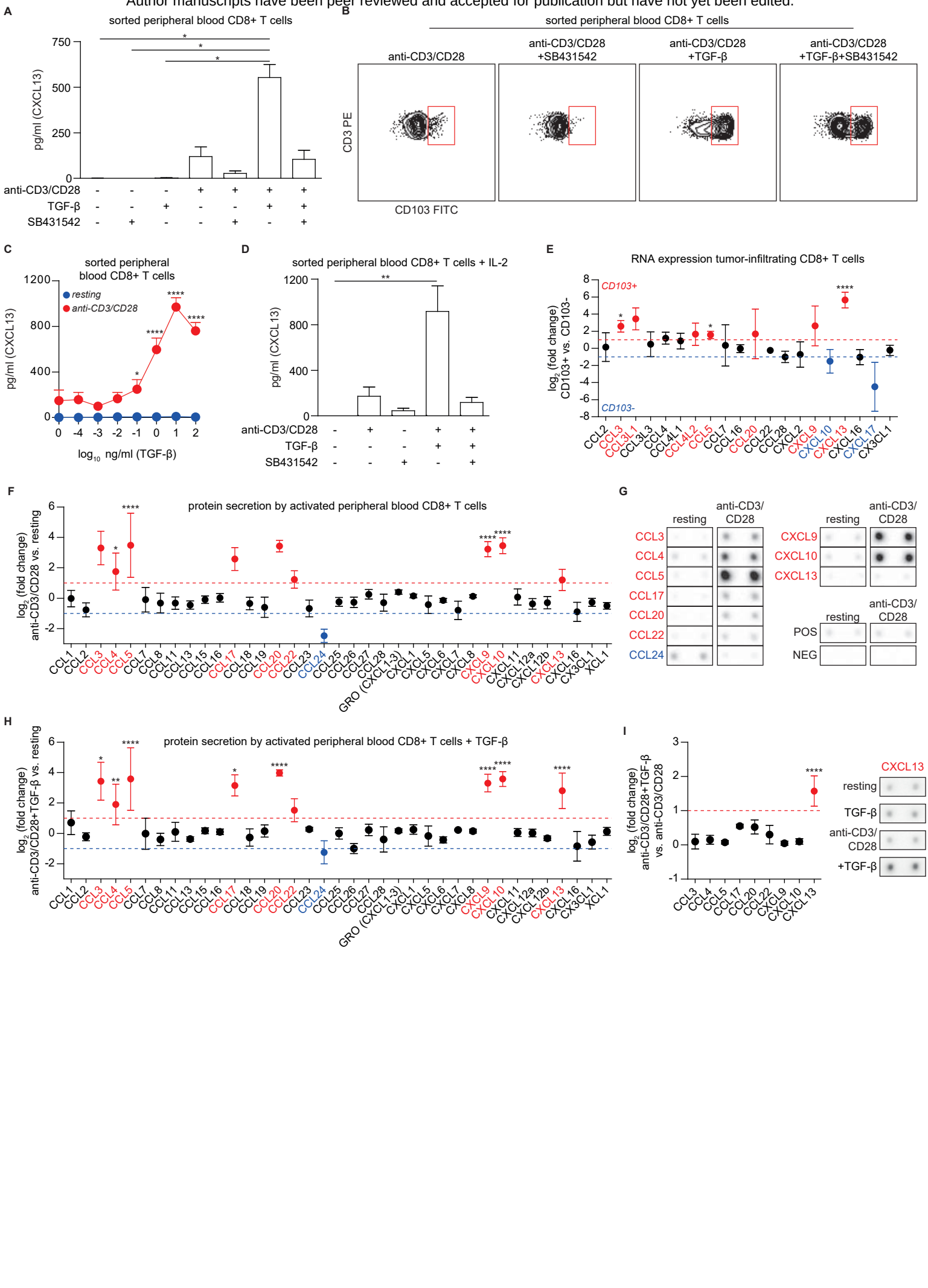

Figure 3
Author Manuscript Published OnlineFirst on March 14, 2019; DOI: 10.1158/2326-6066.CIR-18-0517
Author manuscripts have been peer reviewed and accepted for publication but have not yet been edited.

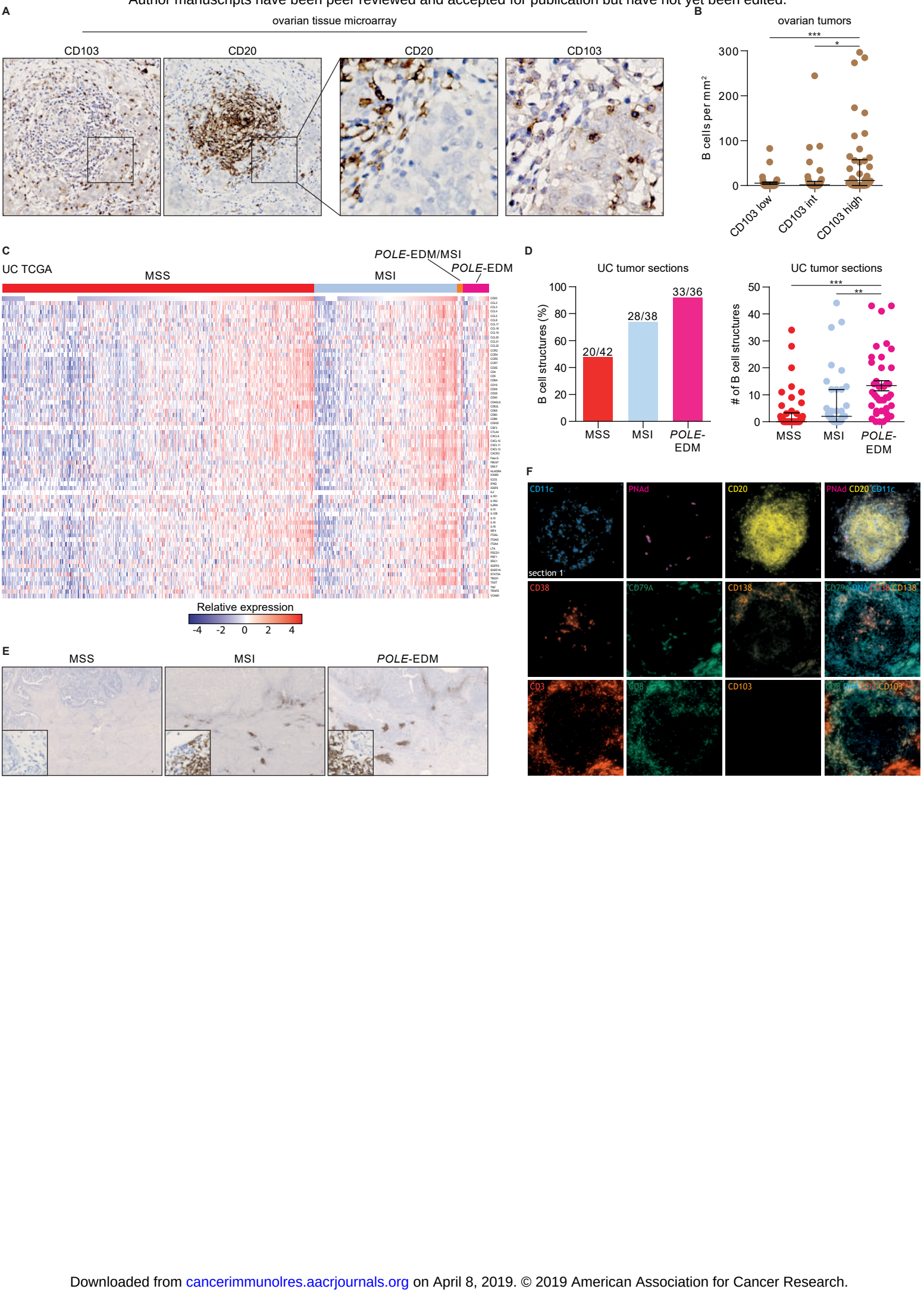

Author Manuscript Published OnlineFirst on March 14, 2019; DOI: 10.1158/2326-6066.CIR-18-0517
Author manuscripts have been peer reviewed and accepted for publication but have not yet been edited.

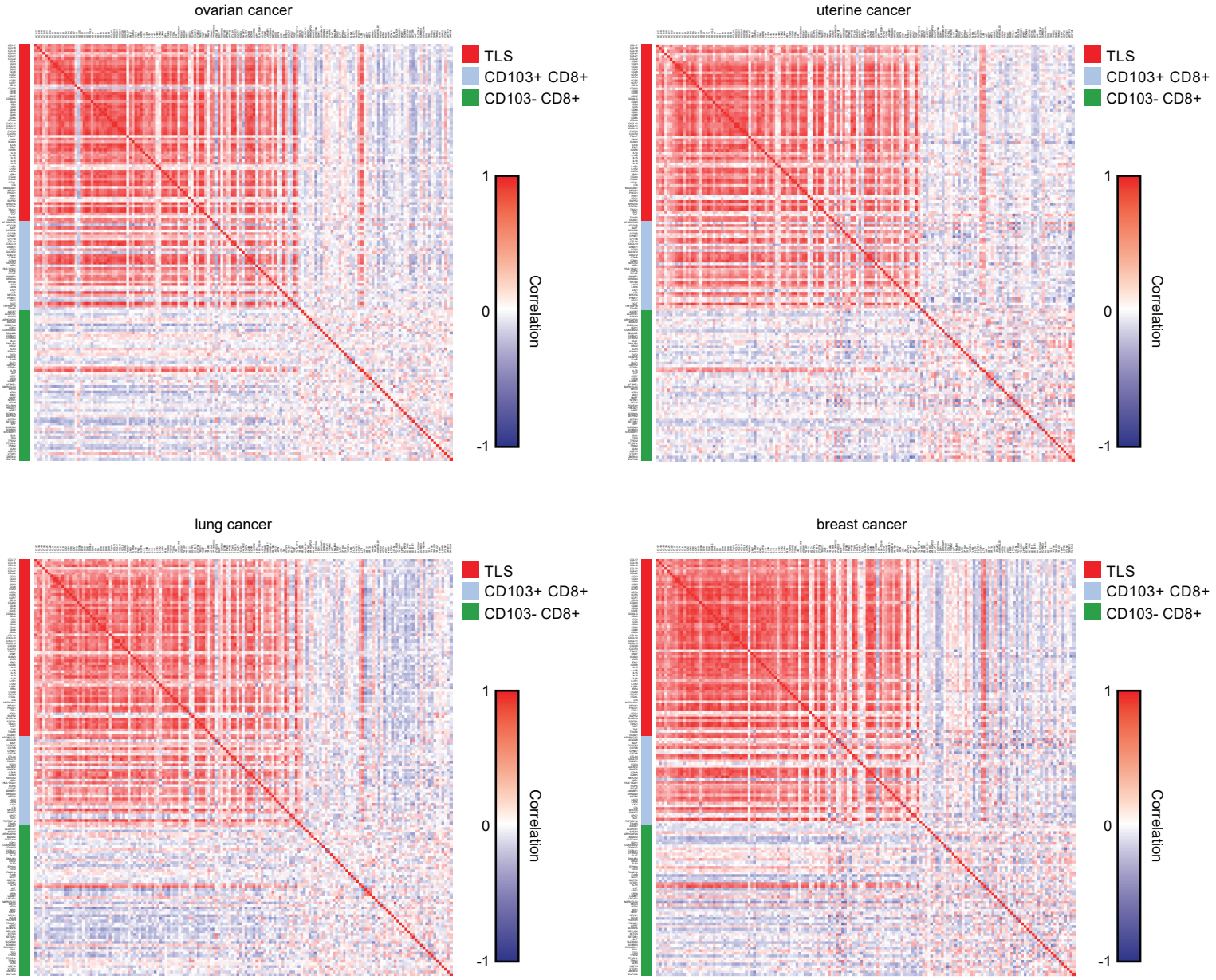

AACR American Association for Cancer Research

Cancer Immunology Research

A transcriptionally distinct CXCL13+CD103+CD8+ T-cell population is associated with B-cell recruitment and neoantigen load in human cancer

Hagma H Workel, Joyce M Lubbers, Roland Arnold, et al.

Cancer Immunol Res Published OnlineFirst March 14, 2019.